



Automatic 3D Mapping for Tree Diameter Measurements in Inventory Operations

Jean-François Tremblay, Martin Béland, François Pomerleau,
Richard Gagnon and Philippe Giguère

EasyChair preprints are intended for rapid dissemination of research results and are integrated with the rest of EasyChair.

July 12, 2019

Automatic 3D Mapping for Tree Diameter Measurements in Inventory Operations

Jean-François Tremblay*, Martin Béland⁺, François Pomerleau*, Richard Gagnon[†], Philippe Giguère*

Abstract Forestry is a major industry in many parts of the world. It relies on forest inventory, which consists of measuring tree attributes. We propose to use 3D mapping, based on the iterative closest point algorithm, to automatically measure tree diameters in forests from mobile robot observations. While previous studies showed the potential for such technology, they lacked a rigorous analysis of diameter estimation methods in challenging forest environments. Here, we validated multiple diameter estimation methods, including two novel ones, in a new varied dataset of four different forest sites, 11 trajectories, totalling 1458 tree observations and 1.4 hectares. We provide recommendations for the deployment of mobile robots in a forestry context. We conclude that our mapping method is usable in the context of automated forest inventory, with our best method yielding a root mean square error of 3.45 cm for our whole dataset, and 2.04 cm in ideal conditions consisting of mature forest with well spaced trees.

Key words: Forestry, Mapping, LIDAR, ICP

1 Introduction

Forestry is an important industry in many countries. In 2016, it accounted for about 13 billion USD in Canada's economy and a similar figure in Sweden's exports of wood products. Yet, worker shortages and high turnover rates coupled with long training time are threatening many operations in this industry. Recent progress in field robotics, such as 3D mapping, have the potential to improve forestry opera-

* Northern Robotics Laboratory, Université Laval

+ Department of Geomatics Sciences, Université Laval

† Centre de Recherche Industrielle du Québec

Communication e-mail: jean-francois.tremblay.36@ulaval.ca

tions while reducing demand for labor. Furthermore, these 3D mapping technologies could be used to estimate wood biomass for carbon accounting purposes [1]. From a scientific point of view, studying the wider context of field robotics in forests is interesting, from the new challenges it generates. For instance, localization and mapping is more difficult in unstructured environments [2].

A key component in modern forest operations is forest inventory [3]. It consists in identifying specific attributes of trees. Some of these attributes, such as species, can be estimated using cameras and advanced computer vision techniques [4]. Others, such as tree diameters, can be extracted from lidar point clouds, as they contain metric information. We conjecture that the ability for an autonomous system to process geometric information via 3D mapping is one of the key elements to the development of future intelligent forest machinery. In our immediate case of forest inventory, this would enable automatic or computer-assisted tree selection for forest harvesting equipment. At the moment, deciding which trees to harvest in a partial cut scenario is performed manually by a technician. This operation has been identified as expensive, time consuming as well as yielding different results depending on the technician [5]. We believe that this could be addressed by equipping harvesting machinery with the proper sensors and algorithms.

This paper explores the use of automatic map building with a standard set of robotic sensors, within the context of forest inventory. Although full 3D maps are produced in the process, as shown in Figure 1, we limit our quantitative study on a single standard attribute in the forest inventory: diameter at breast height (DBH) measurements. The DBH is arguably the most important tree characteristic used for tree selection and wood volume prediction in the forest industry [6]. Typical requirements for diameter measurement accuracy are around 2 cm of error [3], but can be as high as 5 cm for American diameter classes [7]. Early work on tree diameter estimation from lidars focused on terrestrial laser scanning (TLS) [3]. The TLS, which is mounted on a tripod, is manually moved by an operator. Once the individual scans are registered using markers manually installed in the environment, one obtains a very precise 3D map of the environment. However, this data collection approach is significantly more tedious and time consuming than mobile mapping techniques.

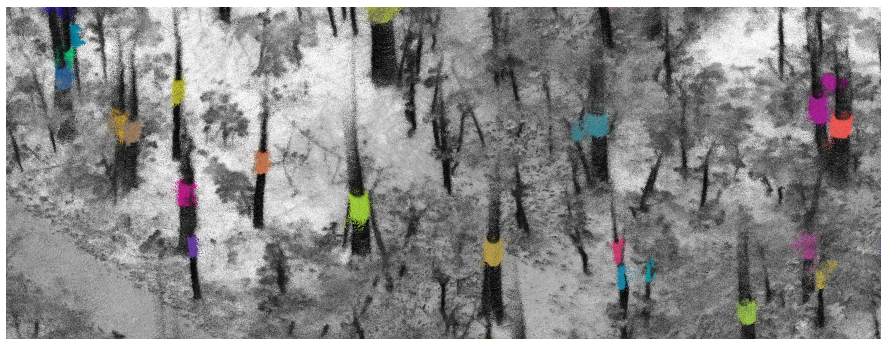


Fig. 1: Perspective view of a forest continuously mapped by a ground vehicle equipped with a 3D lidar, using the method described in Section 3.1. Our focus is on how to best estimate the diameter at breast height, which is highlighted in an individual color for each tree in this figure.

We propose to use an Iterative Closest Point (ICP) 3D mapping approach for forest mapping. A map in 2D might not be sufficient for forest mapping or forest robotics in general. Indeed, forests are rarely flat and even when they are, obstacles on the ground will result on the robot not being levelled, as will be shown in our dataset. Our dataset will present one particularly steep forest where it is not clear how any 2D approach could work. Point clouds generated from this approach tend to be noisier than TLS in nature [3]; this causes problems in the accuracy of diameter extraction. From the generated 3D maps, we automatically estimate tree diameters, comparing several approaches. We validate our complete approach on an extensive dataset of 11 trajectories through four forests, varying topographies, ages, species compositions and densities.

Our contributions are as follows: (1) we test ICP mapping in different forest types for the first time and provide insight about its performance and limitations; (2) we propose a new robust approach to diameter at breast height (DBH) estimation, based on the median of several cylinder fittings, designed to perform well on noisy maps, including those built with ICP; (3) we perform extensive validation of different tree diameter estimation methods from noisy lidar data, and identify which ones perform best; and (4) we provide recommendations on trajectories and field deployment for diameter estimation from robot mapping.

2 Related works

Before measuring tree DBHs from lidar-equipped mobile platforms, one needs to create a map from the observations. Jagbrant et al. [8] used a 2D lidar, combined with GPS and a IMU only for localization, to detect trees in orchards. This approach is not optimal in natural forests as GPS performance is affected by heavy forest canopy. Tsubouchi et al. [9] bridged the gap to natural forests, using a 2D lidar on a pan-tilt unit combined with a tripod. The scans were taken in a static manner as opposed to a moving robot. The mapping was done using a combination of the tree's location and ICP. Tang et al. [10] created maps using Simultaneous Localization and Mapping (SLAM), for trajectories traveling on a road through the forest as opposed to inside the forest itself. This trajectory was selected to improve GPS reception. Importantly, they did not perform full 3D mapping which, as we claim, is key to enabling robotics in forests. Bauwens et al. [11] performed an extensive comparison between a commercial GeoSLAM handheld scanner and TLS. Their testing was limited to circular plots with 15 m radius. They also noted that the SLAM still failed on two of the forest plots tested. More recently, Seki et al. [12] scanned a forest with a 2D lidar and a pan-tilt unit on a backpack, using a SLAM technique called LOAM [13]. Other work using graph-SLAM has been done in [14].

After generating a 3D map, one needs to use either a circle fitting or cylinder fitting algorithm to estimate DBHs. McDaniel et al. [15] presented a method to detect and segment trees in static lidar scans. They tested diameter estimation using cone and cylinder fitting for five sites. They reported a root mean square error (RMSE) of

more than 13 cm, which is not sufficiently accurate for forest inventory. Tsubouchi et al. [9] performed least square 2D circle fitting for diameter estimation. Bauwens et al. [11] used Computree [16] for terrain height models and diameter measurements, which was developed for TLS. Seki et al. [12] employed “the Point Cloud Library RANSAC cylinder fitting method”. In [14], two circle fitting methods were validated: the Pratt fit [17] and least square circle fitting.

Another important aspect is the rigorous analysis of the mapping and diameter extraction method, both in terms of forest variety and the number of trees tested. McDaniel et al. [15] had five test sites, containing 113 trees. In [9], testing was done in one forest with no branches or vegetation-occluding trunks, validating against nine measured trees. Bauwens et al. [11] had the most complete dataset, with 10 test sites consisting of a circle of 15 m radius containing a total of 331 trees. While Tang et al. [10] did not assess their DBH measurements, they measured the position of 224 trees with a total station along one trajectory. While the results in [12] were encouraging, the validation was conducted on one forest site with seven reference trees. [14] evaluated their work in one site under near-perfect conditions; no branches occluding the stem and no ground vegetation causing occlusion.

3 Methods

We describe here our data processing pipeline, starting with map generation, tree segmentation and determining breast height. Finally, we present our different diameter estimation algorithms.

3.1 Iterative closest point mapping

Our 3D mapping method relies on a modified version of `ethz-icp-mapping` [18], which uses the ICP algorithm as the registration solution. ICP takes as input a reading point cloud $\mathbf{Q} \in \mathbb{R}^{3 \times m}$ (i.e., the current lidar view of the robot) containing m points, a map point cloud $\mathbf{M}' \in \mathbb{R}^{3 \times l}$ containing l points, and an initial pose estimate $\hat{\mathbf{T}} \in \text{SE}(3)$ to estimate the pose of the robot in the map. To compute the initial estimate, we used an extended Kalman filter (EKF) to fuse our inertial measurement unit (IMU) and wheel odometry. Reading point clouds are filtered for dynamic elements and maps are uniformly downsampled to keep computation time reasonable. The mapping was not performed in real time, as we prioritized map quality over computation time. The algorithm is described in [Algorithm 1](#).

Algorithm 1 The ICP mapping algorithm used in this paper.

```

1: procedure MAPPING(point clouds  $\mathbf{Q}_{0:t}$ , odometry  $\mathbf{O}_{0:t}$ )
2:    $\mathbf{T}_0 \leftarrow \mathbf{1}$  ▷ Initial pose is at the origin, no rotation
3:    $\mathbf{M}'_0 \leftarrow \text{inputFilters}(\mathbf{Q}_0)$  ▷ Initial map, compute normals
4:   for  $i = 1..t$  do
5:      $\hat{\mathbf{T}}_i = \mathbf{O}_{i-1}^{-1} \mathbf{O}_i \mathbf{T}_{i-1}$  ▷ The initial estimate is the last pose combined with odometry
6:      $\mathbf{Q}'_i = \text{inputFilters}(\mathbf{Q}_i)$  ▷ Compute normals
7:      $\mathbf{T}_i = \text{icp}(\mathbf{Q}'_i, \mathbf{M}'_{i-1}, \hat{\mathbf{T}}_i)$  ▷ Refine pose estimate with ICP
8:      $\mathbf{M}_i = (\mathbf{M}'_{i-1} \mid \mathbf{T}_i \mathbf{Q}'_i)$  ▷ Add points to map
9:      $\mathbf{M}'_i = \text{reduceDensity}(\mathbf{M}_i)$  ▷ Aim for a density of one point per  $8 \text{ cm}^3$ 
10:  end for
11:  output final map  $\mathbf{M}'_t$  and trajectory  $\mathbf{T}_{0:t}$ 
12: end procedure

```

3.2 Point selection for DBH estimation

The first step in estimating DBH from a 3D map is to segment trees. Although automatic methods exist [15, 16], we chose to perform the tree segmentation manually. Our motivation is to validate diameter estimation methods also on less visible trees regardless of segmentation quality. Our manual segmentation comes in the form of 3D bounding-boxes around trunks, which were manually adjusted. These bounding-boxes can include branches and noise, which will be outliers stressing the DBH estimation methods.

To estimate the DBHs, we had to locate the breast height of each tree, defined as 1.3 m above ground level. This implies estimating the ground level at each tree location in the point cloud using a digital terrain model (DTM). Several algorithms have been designed for this purpose [15], from which we chose the raster-based method. The ground height for a given tree was the value of the DTM given the (x, y) position of the center of the manually drawn bounding box. Then, we selected every point in the tree bounding box which was between $h/2$ below breast height and $h/2$ above, where h represents a section thickness. Selecting this thickness h was a trade-off between inducing an error from the change in diameter along a tree's height and the fact that cylinder fitting performs better as more points are available. Points resulting from this selection are colored in Figure 1. Those points were finally used to estimate the DBH by one of the cylinder fitting methods described below.

3.3 Least square cylinder fitting

As commonly done [12, 15, 16], we formulate tree diameter estimation as cylinder-fitting. Fitting cylinders to point clouds is a fairly well studied problem [19]. Let $\mathbf{P} = (\mathbf{p}_1 \ \mathbf{p}_2 \ \dots \ \mathbf{p}_n) \in \mathbb{R}^{3 \times n}$ be the slice in our point cloud described in Section 3.2 and containing n points belonging to one tree. We also have $\mathbf{N} = (\mathbf{n}_1 \ \mathbf{n}_2 \ \dots \ \mathbf{n}_n) \in \mathbb{R}^{3 \times n}$, which are the surface normals for each \mathbf{p}_i . We used the spectral decomposition of

the covariance matrix from the q -nearest neighbors for each \mathbf{p}_i to estimate \mathbf{N} . The eigenvector associated with the smallest eigenvalue of this matrix is the direction of least variance, corresponding to the estimated normal of the surface. A cylinder used to fit \mathbf{P} can be represented in multiple ways. For this work, we parametrize a cylinder as $(\mathbf{a}, \mathbf{c}, r)$ where $\mathbf{a} \in \mathbb{R}^3 : \|\mathbf{a}\|_2 = 1$ is the cylinder axis direction, $\mathbf{c} \in \mathbb{R}^3$ is any point on the cylinder axis and $r \in \mathbb{R}^+$ is the cylinder radius. This parametrization has seven parameters, with one degree of freedom removed from the axis norm constraint; the last degree of freedom can be removed by imposing $\mathbf{a} \cdot \mathbf{c} = 0$ which comes naturally when solving for \mathbf{c} in the next cylinder fitting method presented. From there, we investigated four methods to find those parameters from the point cloud \mathbf{P} .

1) Finding the axis using surface normals — The *linear least square* method (A_{LLS}) [20] needs the surface normals \mathbf{N} . This axis-finding method is based on the fact that if \mathbf{P} and \mathbf{N} represent a perfect cylinder, then all normals $\mathbf{n}_i, i = 1 \dots n$ will lie on a plane passing through the origin for which the normal will be \mathbf{a} . Therefore, finding the optimal axis \mathbf{a}^* for a cylinder can be done by solving

$$\mathbf{a}^* = \arg \min_{\mathbf{a}} \|\mathbf{N}^\top \mathbf{a}\|_2. \quad (1)$$

As it turns out, \mathbf{a}^* is the third right singular vector of the singular value decomposition of the matrix \mathbf{N} . A useful property of the A_{LLS} method is that it is linear. We can then project \mathbf{P} on a plane perpendicular to \mathbf{a}^* ; the resulting 2D point cloud can be used to fit a circle using any known method discussed in the next paragraph. This circle fitting method will find the remaining parameters r and \mathbf{c} . Another approach (A_N) in finding the cylinder axis is assuming that the tree is perfectly vertical, leading to the simplification $\mathbf{a} = (0 \ 0 \ 1)$. This approach was employed in [9, 14].

2) Circle fitting algorithms — Once the axis \mathbf{a} of a cylinder is known, one can project the points in \mathbf{P} on a plane perpendicular to this axis and then fit a circle to find the radius r and center \mathbf{c} . This can be done using *iterative* or *algebraic* methods. The iterative methods consist of minimizing the sum of squares of the point-to-circle distance using iterative methods. Consequently, they are prone to local minima issues. The algebraic methods do not rely on iterative methods, but rather analytically solve the problem of circle fitting using an approximation of point-to-circle distance [17]. In our experiments, we used an algebraic fit called *Hyper*, abbreviated as H , introduced in [21]. In their paper, the authors prove that they have a non-biased fit, as opposed to Pratt [17], in the case of incomplete circle arcs.

3) Non-linear least square cylinder fitting — This method, presented by Lukács et al. [19], uses non-linear optimization to estimate the complete cylinder parameters. It relies on a point-to-cylinder distance: $d(\mathbf{p}_i; \mathbf{a}, \mathbf{c}, r) = \|(\mathbf{p}_i - \mathbf{c}) \times \mathbf{a}\|_2 - r$. To find the cylinder, one then solves

$$\mathbf{a}^*, \mathbf{c}^*, r^* = \arg \min_{\mathbf{a}, \mathbf{c}, r} \sum_{i=1 \dots n} d^2(\mathbf{p}_i; \mathbf{a}, \mathbf{c}, r) + \underbrace{\sum_{i=1 \dots n} (\mathbf{n}_i \cdot \mathbf{a})^2}_{\text{Normals loss (optional)}}. \quad (2)$$

The second sum is optional, but can be added to the minimization to penalize cylinders which do not fit \mathbf{N} well. To the best of our knowledge, this penalty has not been described elsewhere in the literature. For this paper, the original method without normals will be called C_{NLS} , while the minimization with the extra penalty will be

called C_{NLSN} . We can solve this optimization problem in an unconstrained manner, by converting the problem to the cylinder parametrization from Lukács et al. [19].

4) Multiple cylinders voting — We can fit multiple cylinders to the tree slice to improve the estimate robustness. In this case, we divide our tree slice vertically to form n_{cyls} point clouds, and fit a cylinder to each one. Then, one can choose the median (V_{median}) or the mean (V_{mean}) of the diameter of the cylinders as the DBH.

4 Experimental Setup

For each tree in our test sites, a forest technician identified all species and measured the diameter of trees using a specialized diameter tape. This information was engraved on a small metal marker attached to each tree. The only criteria for tree inclusion in the dataset was that (1) its diameter was greater than 2 cm and (2) the tree was standing. We generated initial 3D maps from our robot observations, and then segmented every individual tree in these maps, assigning an ID to each tree. Afterwards, a stem map (i.e., a two-dimensional plot of the position of every individual tree and its ID) was generated and printed on paper. We then used this stem map in the field to associate each tree to its ID, and then recover the measurement made by the technician. Unfortunately, even differential GPS cannot be used to localize trees sufficiently precisely for this task, due to canopy interference. In the end, the information for each tree included (1) an individual ID, (2) its position in the 3D map in the form of a bounding box, (3) its ground-truth DBH, and (4) its species.

We used a *Clearpath Husky A200* mobile robot to map the different forest sites. Its skid drive makes it appropriate for navigating rough forested environments and emulating forest machinery. The robot was equipped with a *Velodyne HDL32* lidar, an *Xsens MTI-30* IMU and wheel encoders for odometry. All processing was performed offline on a workstation with an AMD Ryzen 1700 and 64 GB of RAM.

4.1 Experimental sites

We collected data on four significantly different sites, scanning in total 1.4 hectares. We manually measured and marked 943. From these, 588 were above 10 cm in DBH (trees below this threshold are not considered of commercial value) and kept for our study. We chose sites that were different in terms of age, composition (see [Figure 3](#)), density and topography (see [Figure 2](#)), to identify how these factors could affect our diameter estimation and robot mapping. The first three sites were located at Forêt Montmorency, owned by Laval University. The last one was located on the University campus, as Forêt Montmorency contains little deciduous forest. We tested a number of trajectories for each site, to see their impact on diameter estimation. The different trajectories were placed in a common coordinate system for each site, using the approach proposed in [22]. For our analysis, each tree observed in a given



Fig. 2: Photos of our test sites. One can see the variety in composition and density; from tightly planted balsam firs in YOUNG to well spaced mature spruce in MATURE. Also visible is the rough ground of YOUNG and MATURE, compared to that of MIXED and MAPLE.

trajectory is considered as an individual tree observation. Therefore, we have in our dataset 2 to 4 observations for each tree. By far, these four sites represent the largest DBH dataset from mobile lidar in the literature. We describe them below.

1) Young balsam firs (YOUNG) — Despite being a plantation, the topography of this site was very rough, with a 30 % incline and mossy soil. The robot experienced frequent slippage, thus affecting odometry. There were a lot of lower branches occluding the trunks at breast height, which could affect our measurements. The trees were tightly planted, resulting in reduced visibility for the lidar. These factors make this site challenging both for perception and navigation. This site was mostly composed of balsam firs with some paper birch and measured $30\text{ m} \times 35\text{ m}$. Two trajectories were performed on this site: one big loop around the site, and a longer one where we made a loop around the site but also crossed the site in the middle.

2) Mixed boreal forest (MIXED) Despite being generally flat, this site had a lot of branches on the ground, making navigation difficult. The understory vegetation was also very dense in some places, thus limiting visibility. It was diverse in terms of tree species and age, consisting mainly of quaking aspens, balsam firs and spruce. The site was $50\text{ m} \times 30\text{ m}$. We conducted three trajectories: the first one was a simple loop around the site, while the other two tried to be more exhaustive.

3) Mature boreal forest (MATURE) There was a 10 % incline, not as sharp as YOUNG, and very irregular ground. This site had big trees with non-occluded trunks. Being a mature forest, there was a fair number of fallen trees which could block the robot. The site was mostly composed of balsam fir as well as white and black spruce. This site measures $30\text{ m} \times 40\text{ m}$. Two trajectories were performed, similarly as in YOUNG.

4) Mature natural maple forest (MAPLE) It was flat and easy to navigate, with very few obstacle on the ground. Consequently, we drove the robot at a faster speed (1 m/s) for much of the trajectories. It was a mature deciduous natural forest, com-

posed mainly of sugar and red maple. The site was $100\text{ m} \times 100\text{ m}$ and contained upwards of 1000 trees. To reduce the ground-truth labor, we randomly selected 100 trees which we would measure. Two trajectories, similar to YOUNG and MATURE, were performed at the beginning of October with the leaves on the trees. The same trajectories were repeated at the beginning of November with no leaves left, to study the potential impact of leaves on diameter estimation.

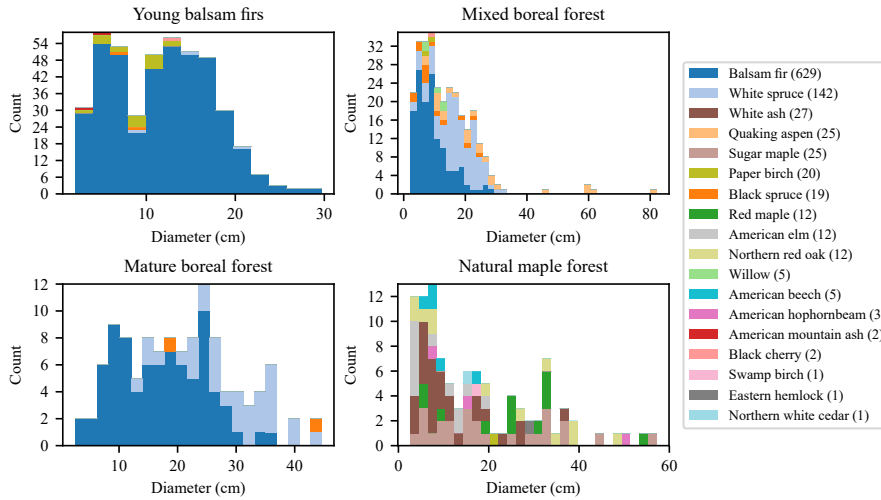


Fig. 3: Diameter and species distribution for our test sites, with the tree count by species in parenthesis. Notice the species and diameter diversity in the different sites. This allowed us to verify the impact of species on diameter estimation, as bark texture impacts the point cloud produced by the lidar. Trees of less than 10 cm were segmented and measured, but were not used in this paper.

5 Results and discussion

5.1 Comparing diameter estimation approaches

We tested different combinations of the methods presented in Section 3.3, to determine the best one. First, we tested the combination of A_N and H , which can be summarized as fitting a circle to the xy -coordinates of the tree slice. Similarly, we tested A_{LLS} and H . Also, we tested combining both methods above with C_{NLS} and C_{NLSN} , using both of the first as initial estimates for the two later. All six resulting methods were combined with either V_{median} and V_{mean} , resulting in 12 sets of results. All combinations used RANSAC as the outlier rejection method, with tolerance ϵ . We limited this comparison for trees observed at a distance closer than 10 m. As will be shown in Section 5.2, this minimal observation distance has too large of an im-

pact on the estimation of DBH, and we consider accurate DBH measurement from this distance currently unfeasible. This meant discarding 143 out of our 1458 tree observations. We tested all of the following hyperparameter values: $q \in \{15, 20, 25\}$, $n_{cyls} \in \{1, 2, 3, 4, 5\}$, $h \in \{20, 30, 40, 50, 60\}$ cm, and $\varepsilon \in \{1, 2, 3\}$ cm.

Because V_{mean} consistently underperformed V_{median} in all of our tests, its performance is not reported in [Table 1](#). The inferior performance of V_{mean} was also confirmed by the fact that the number of vertical slices $n_{cyls} = 1$ was always the best choice in our hyperparameters exploration with V_{mean} , meaning that not using V_{mean} was preferable to using it.

Table 1: Results of our diameter estimation methods combined with V_{median} on our dataset (11 trajectories on four sites). The fail rate is the proportion of trees where there were not enough points, or the error was above 20 cm. We treated those failures as outliers; they were not used to compute the RMSE or bias. The result shown for each method was computed using the best combination (in terms of RMSE) of hyperparameters. Because *Hyper* is used for all of the methods, it is removed from the first row.

	A_{LLS}	A_N	$A_{LLS} + C_{NLS}$	$A_N + C_{NLS}$	$A_{LLS} + C_{NLSN}$	$A_N + C_{NLSN}$
RMSE (cm)	5.08	4.41	3.76	3.45	3.86	3.66
Bias (cm)	-0.95	0.72	-0.62	-0.41	-0.18	0.00
Fail rate (%)	11.41	13.61	6.23	6.46	6.54	7.53
q	25	<i>N/A</i>	25	<i>N/A</i>	25	20
n_{cyls}	1	3	5	5	3	5
h (cm)	20	60	60	60	40	50
ε (cm)	3	3	2	2	2	1

Legend: A_{LLS} —lin. l.-s. axis, A_N —vertical axis, C_{NLSN} —non-lin. l.-s. with normals, C_{NLS} —without normals.

One can see that the best performing method is $A_N + C_{NLS}$ and that the worst is A_{LLS} . One conclusion from our comparison is that V_{median} leads to better results. All of the methods, except A_{LLS} , performed better when n_{cyls} was larger than one. Surprisingly, using a pure vertical tree axis (A_N) performed better than trying to take into account the stem direction (A_{LLS}), even as an initial estimate to non-linear cylinder fitting. This suggests that A_{LLS} is not precise enough to estimate the stem direction accurately in noisy mobile lidar point clouds. However, the vast majority of our trees grew vertically in our dataset, thus there may be a bias favoring A_N .

Our best performing site was MATURE, with its well-spaced trees and visible trunks. [Figure 4](#) gives an example of the error distribution achieved in one trajectory with $A_{LLS} + H + C_{NLSN} + V_{median}$ in these ideal circumstances.

5.2 Factors impacting DBH estimation

The following statistics were generated using the $A_N + H + C_{NLS} + V_{median}$ method, but similar observations can be made for others. We tried to identify possible factors impacting the estimation of DBH. For instance, we can see in [Figure 5](#) the impact of minimal observation distances and presence of foliage on the error distribution,

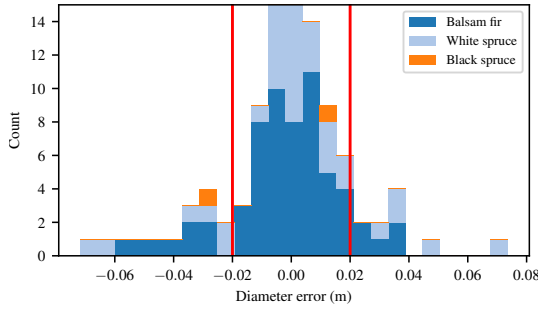


Fig. 4: Error distribution over 94 trees for our best performing site, MATURE, using the second trajectory. In red is the 2 cm error limit. Overall, the RMSE is 2.16 cm, the bias is 0.15 cm, and the RMSE of trees observed closer than 8 m (all but 4 trees, which are at the tail ends of the distribution is this figure) is 2.04 cm. The hyperparameters for these results were $\epsilon = 1$ cm, $h = 40$ cm, $n_{cyls} = 3$ and $q = 15$.

for the MAPLE dataset. This minimal observation distance represents how close the robot was driven from a tree. We observe that the error becomes too high (i.e., more than 10 cm of RMSE) for trees to which the robot has not gotten closer than 10 m, particularly when trees have foliage; again, this is similar for the other three sites. The effect of foliage could be due to increased localization error incurred during the map creation process of [Section 3.1](#) or reduced trunk visibility.

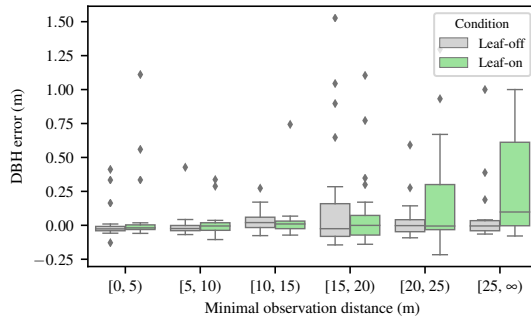


Fig. 5: Error vs. minimal observation distance for MAPLE. We can see that the error spread (in terms of interquartile ranges) is higher in leaf-on conditions, from 0 to 10 m of observation distance. After 10 m, the error becomes too great for forest inventory purposes. Note the degradation after 20 m in leaf-on conditions, due to the lack of points.

We also observed that the localization error can result in a reduced diameter estimation accuracy. In MATURE, the trajectory that looped around the site resulted in significant localization error, as stem sections of the same trees observed at the beginning of the trajectory were misaligned with observations made at the end of the trajectory. This caused a bias of -1.01 cm for the loop, while the other two trajectories had a respective bias of -0.31 cm and 0.03 cm. This trajectory was the only one in our dataset with such visible localization error.

Finally, another factor impacting the estimation of DBH is species, which we attributed to the influence of bark roughness. For example, the big red maples in MAPLE had a bias of -5 cm, the quaking aspens of MIXED had a bias of -1.61 cm while the very smooth balsam firs overall had limited bias (0.47 cm), after removing the results from the problematic trajectory mentioned above. The same effect of bark texture on DBH measurements has also been observed by Bauwens et al. [11].

5.3 *Lessons learned*

During the course of this work, we gained significant experience in field deployment of mobile robots in forests. Here are some lessons and recommendations that could be useful to anyone interested in deploying robots in forests for 3D mapping and inventory purposes, as well as more sophisticated experiments where observing trees is important.

- Ground roughness, such as branches, irregular ground or other obstacles, did not seem to have a significant impact on our mapping and diameter estimation, as our two best performing sites, MATURE and YOUNG, were also the ones where the robot had the most trouble navigating.
- Getting close to each tree is essential for DBH estimation: our experiments show that diameter estimation performance degrades rapidly for observations beyond 6 m and becomes unusable after 10 m. This could be due to propagation of the orientation estimation error during the map building process, lidar beam width or point density reduction. In each site, more exhaustive trajectories always performed better than simple loops. For example in MIXED, we even observed a negative bias caused by localization error in the simple loop.
- Our results in MAPLE were affected by the robot speed. At 1 m/s, the platform moves 10 cm during each lidar scan, which is ignored by ICP. This limitation of the algorithm led to poorer results in what, we thought, should have been the best performing site. Solving this issue by inferring the movement of the platform during one scan, such as done by Zhang and Singh [13], is important if we want this approach to work in fast moving forest robots. It would also allow for faster data acquisition, as well as possibly lead to more accurate DBH estimation overall.
- Mobility in forests is challenging; we pushed our robot to its limit. Using continuous tracks would be ideal, as it is used for most forest machinery. In MATURE we had to slightly alter the environment for our robot by cutting three fallen trees (which are abundant in mature forests), while other sites were navigable with no modifications. From a pure forest inventory standpoint, a backpack-mounted or handheld sensor system would be better suited, but it remains interesting nonetheless to study robot perception in such difficult conditions.

6 Conclusion

In this paper, we presented an ICP mapping approach in forests, and demonstrated that it produced maps that were accurate enough to perform tree diameter estimation, especially in mature, well-spaced forests where we reached an accuracy of 2.04 cm. We also identified key challenges to address in robot mapping in forests: dealing with rough tree bark, reduced visibility in dense forest and estimating platform motion during one scan. We compared multiple diameter estimation methods,

and concluded that fitting multiple cylinders using *Hyper* circle fitting combined with non-linear cylinder fitting, and taking the median of the diameters of those cylinders works best. All of our methods were validated in the most extensive dataset of DBH measurement from mobile lidar in the literature.

6.1 Future work

3D mapping opens the door for future automation of forestry equipment. The next step would be localizing a forest harvester in our 3D point cloud in real time. More work is needed in this direction as we did not attempt getting our mapping algorithm to run in real time while producing maps that were accurate enough to measure the DBH of trees. Trying to use trees as landmarks to take some pressure off ICP could be a solution. Furthermore, integrating work by Carpentier et al. [4] to perform species classification would be beneficial for tree selection applications. Although we restricted our evaluations on DBH estimation and not quality of the maps, note that the latter can play an important role in other automated tasks such as navigation and tree grasping. Evaluating the possible use of our maps for these purposes would be of interest. While we did not attempt to measure trees whose DBH was less than 10 cm, there is interest in being able to detect and measure those small trees for regeneration monitoring purposes, as well as to avoid damaging them during operations. More work is needed to achieve accurate measurement of those small trees from mobile lidar. Such accuracy could possibly be achieved by combining the range measurements of lidar with angular measurements made with a camera.

Acknowledgements This work was supported by a Mitacs Accelerate grant and FORAC. We thank the Canadian Space Agency for lending us their Velodyne HDL-32, the Forêt Montmorency staff, especially Charles Villeneuve, for his help with tree measurements as well as Simon-Pierre Deschênes and Philippe Dandurand for their help with field work.

References

- [1] K. Calders, G. Newnham, A. Burt, et al. Nondestructive estimates of above-ground biomass using terrestrial laser scanning. *Methods Ecol. Evol.*, 6(2): 198–208, 2015.
- [2] F. Pomerleau, F. Colas, R. Siegwart, et al. Comparing icp variants on real-world data sets. *Auton. Robot.*, 34(3):133–148, 2013.
- [3] X. Liang, V. Kankare, J. Hyypä, et al. Terrestrial laser scanning in forest inventories. *ISPRS J. Photogramm.*, 115:63 – 77, 2016.
- [4] M. Carpentier, P. Giguère, and J. Gaudreault. Tree species identification from bark images using convolutional neural networks. In *IEEE/RSJ Int. Conf. Int. Robot.*, pages 1075–1081, 2018.

- [5] L. Vítková, Á. N. Dhubháin, and A. Pommerening. Agreement in Tree Marking: What Is the Uncertainty of Human Tree Selection in Selective Forest Management? *Forest Sci.*, 62(3):288–296, 2016.
- [6] P. W. West. *Tree and Forest Measurement*. Springer, 2009.
- [7] USDA Forest Inventory and Analysis Glossary. <https://www.nrs.fs.fed.us/fia/data-tools/state-reports/glossary>.
- [8] G. Jagbrant, J. P. Underwood, J. Nieto, et al. Lidar based tree and platform localisation in almond orchards. In *Field and Service Robotics*, pages 469–483. Springer, 2015.
- [9] T. Tsubouchi, A. Asano, T. Mochizuki, et al. Forest 3d mapping and tree sizes measurement for forest management based on sensing technology for mobile robots. In *Field and Service Robotics*, pages 357–368. Springer, 2014.
- [10] J. Tang, Y. Chen, A. Kukko, et al. Slam-aided stem mapping for forest inventory with small-footprint mobile lidar. *Forests*, 6(12):4588–4606, 2015.
- [11] S. Bauwens, H. Bartholomeus, K. Calders, and P. Lejeune. Forest inventory with terrestrial lidar: A comparison of static and hand-held mobile laser scanning. *Forests*, 7(6), 2016.
- [12] S. Seki, T. Tsubouchi, S. Saratat, and Y. Hara. Forest mapping and trunk parameter measurement on slope using a 3d-lidar. In *IEEE/SICE Int. Symp. on Sys. Int.*, pages 380–386, 2017.
- [13] J. Zhang and S. Singh. Loam: Lidar odometry and mapping in real-time. In *Robotics: Science and Systems*, Berkeley, USA, 2014.
- [14] M. Pierzchała, P. Giguère, and R. Astrup. Mapping forests using an unmanned ground vehicle with 3d lidar and graph-slam. *Comput. Electron. Agr.*, 145:217–225, 2018.
- [15] M. W. McDaniel, T. Nishihata, C. A. Brooks, et al. Terrain classification and identification of tree stems using ground-based lidar. *J. Field Robot.*, 29(6): 891–910, 2012.
- [16] A. Othmani, A. Piboule, M. Krebs, et al. Towards automated and operational forest inventories with T-Lidar. In *Int. Conf. LiDAR App. Asses. Forest Eco.*, Hobart, Australia, 2011.
- [17] V. Pratt. Direct least-squares fitting of algebraic surfaces. In *ACM Comp. Graph.*, volume 21, pages 145–152. ACM, 1987.
- [18] F. Pomerleau, P. Krösi, F. Colas, et al. Long-term 3d map maintenance in dynamic environments. In *IEEE Int. Conf. on Robot.*, pages 3712–3719, 2014.
- [19] G. Lukács, R. Martin, and D. Marshall. Faithful least-squares fitting of spheres, cylinders, cones and tori for reliable segmentation. In *Eur. Conf. on Comp. Vis.*, pages 671–686. Springer, 1998.
- [20] L. Li, M. Sung, A. Dubrovina, et al. Supervised fitting of geometric primitives to 3d point clouds. In *IEEE Conf. on Comp. Vis. and Pat. Rec.*, 2019.
- [21] A. Al-Sharadqah and N. Chernov. Error analysis for circle fitting algorithms. *Electronic J. Stat.*, 3:886–911, 2009.
- [22] J.-F. Tremblay and M. Béland. Towards operational marker-free registration of terrestrial lidar data in forests. *ISPRS J. Photogramm.*, 146:430 – 435, 2018.